Deducing Ground-to-Air Emissions from Observed Trace Gas Concentrations: A Field Trial

T. K. FLESCH AND J. D. WILSON

Department of Earth and Atmospheric Sciences, University of Alberta, Edmonton, Alberta, Canada

L. A. HARPER

U.S. Department of Agriculture, Agricultural Research Service, Watkinsville, Georgia

B. P. CRENNA

Department of Earth and Atmospheric Sciences, University of Alberta, Edmonton, Alberta, Canada

R. R. SHARPE

U.S. Department of Agriculture, Agricultural Research Service, Watkinsville, Georgia

(Manuscript received 30 June 2003, in final form 24 October 2003)

ABSTRACT

The gas emission rate Q from an artificial 36-m^2 surface area source was inferred from line-average concentration C_L measured by an open-path laser situated up to 100 m downwind. Using a backward Lagrangian stochastic (bLS) model, a theoretical C_L/Q relationship was established for each experimental trial by simulating an ensemble of fluid-element paths arriving in the laser beam under the prevailing micrometeorological conditions. The diagnosed emission rates (Q_{bLS}) were satisfactory for trials done when Monin–Obukhov similarity theory gave a good description of the surface layer, but were poor during periods of extreme atmospheric stability ($|L| \leq 2$ m) and transition periods in stratification. With such periods eliminated, the average value of the 15-min ratios Q_{bLS}/Q over $n = 77$ fifteen-minute trials spanning 6 days was 1.02. Individual 15-min estimates, however, exhibited sizable variability about the true rate, with the standard deviation in Q_{bLS}/Q being $\sigma_{Q/Q} = 0.36$. This variability is lessened ($\sigma_{Q/Q} = 0.22$, $n = 46$) if one excludes cases in which the detecting laser path lay above or immediately downwind from the source—a circumstance in which the laser path lies at the edge of the gas plume.

1. Introduction

The measurement of gas emissions from the surface to air is a difficult problem. Several meteorological techniques are available (e.g., eddy covariance, flux gradient, integrated horizontal flux), but they involve complex instrumentation (e.g., concentration measurements at many heights, fast-response concentration sensors) and restrictions on the measurement site.[1]

One may sidestep these problems by using an atmospheric dispersion model to deduce the emission rate indirectly. Consider the situation in Fig. 1. An area source of known configuration emits gas at a uniform but unknown rate Q (kg m^{-2} s^{-1}), and a time-average tracer concentration C is measured at point M within the plume. With a model prediction of the ratio of concentration at M to the emission rate $(C/Q)_{\mathrm{sim}}$, one can infer the emission rate as

$$Q = \frac{(C - C_b)}{(C/Q)_{\mathrm{sim}}}, \tag{1}$$

where C_b is the background tracer concentration. This approach is often called ''inverse dispersion modeling,'' because the goal is to deduce source information from known concentrations, rather than the more common practice of deducing concentrations from a known source. Inverse modeling has been applied to a broad range of source-inference problems, from the micrometeorological to the continental scale, from single

[1] Most techniques require a flat and homogeneous location with an extensive and uniform source. An exception is the integrated horizontal flux technique, which is practical for sources with small upwind dimensions and a large crosswind extent.

Corresponding author address: T. K. Flesch, Department of Earth and Atmospheric Sciences, University of Alberta, Edmonton, AB T6G 2E3, Canada.
E-mail: thomas.flesch@ualberta.ca

© 2004 American Meteorological Society

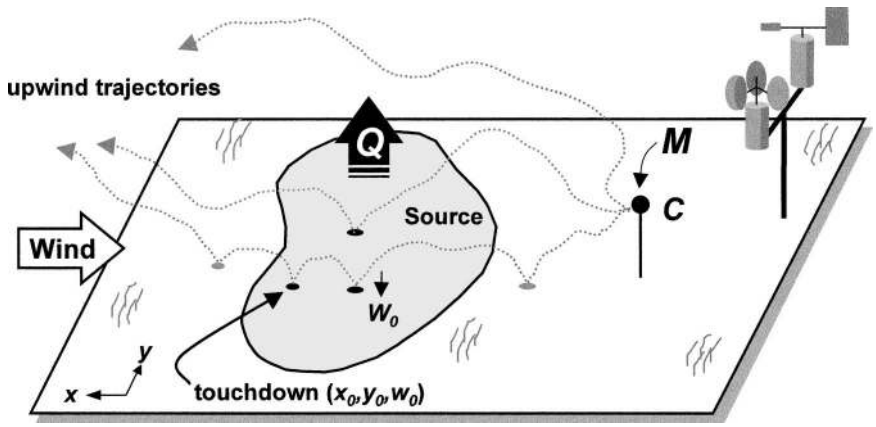

FIG. 1. Illustration of the bLS technique for estimating tracer emission rate Q. Average concentration C is measured at point M downwind of the source. The ratio $(C/Q)_{\mathrm{sim}}$ is calculated from upwind trajectory touchdowns inside the source (w_0 is the vertical velocity at touchdown).

sources to spatially variable source fields, and from chemically reactive to inactive species (e.g., Wilson et al. 1982; Raupach 1989; Carter et al. 1993; Hartley and Prinn 1993; Seibert 1999; Kaharabata et al. 2000).

What are the advantages of the inverse-dispersion method for the kind of problem illustrated in Fig. 1? If the dispersion model accurately mimics atmospheric transport, then there are no fundamental restrictions on the size or shape of the emission source. There is also flexibility in the location of M, which in principle can be anywhere in the emission plume. Any tracer property that can be measured, predicted by a dispersion model, and uniquely related to Q can be used as the basis of the method. For instance, given an instrument to measure line-average concentration C_L, this quantity could be substituted for C so that $(C_L/Q)_{\mathrm{sim}}$ would be the object of model prediction.

Any type of dispersion model could be used to predict $(C/Q)_{\mathrm{sim}}$. More accurate models require specifying spatially and temporally variable wind fields for both the average wind and turbulence—a difficult proposition. However, if one's interest is the horizontally homogeneous surface layer (below a height of approximately 50 m and above a plant canopy), then all needed wind statistics can be determined from a few key surface observations. Monin–Obukhov similarity theory (MOST) posits that the statistical properties of the wind in the surface layer are determined by the momentum and heat fluxes through the layer, as quantified by the friction velocity u_* and the Obukhov stability length L (see Garratt 1992). A full description also requires the wind direction β and surface roughness length z_0.

We can define an ''ideal surface-layer problem'' as needing only u_*, z_0, L, and β to determine $(C/Q)_{\mathrm{sim}}$ accurately. If the source and the detection point M lie within a horizontally homogeneous surface layer and the source-to-M distance is sufficiently short, so that tracer paths remain in the surface layer, application of the inverse-dispersion technique is reasonably straightforward.[2] Many agricultural and environmental source-estimation problems potentially fit this category. These problems may include emissions from small soil research plots, feedlots, ponds, industrial grounds, and so on, that often occur in circumstances for which it is reasonable to assume that the local wind flow is ''tolerably'' uniform[3] (viz., wind statistics that do not deviate more than 10%–20% from their spatial average over the region from source to detector).

This paper describes a field experiment in which the inverse-dispersion technique was used to determine Q in an ideal surface-layer setting. We constructed a small area source from which methane (CH_4) was released at known rates over a wide range in meteorological conditions. An open-path laser measured line-average methane concentration C_L at positions located up to 100 m downwind of this source. A corresponding $(C_L/Q)_{\mathrm{sim}}$ was calculated using a backward Lagrangian stochastic (bLS) dispersion model, and the resulting estimate of the emission rate Q_{bLS} was compared with the known Q. Our objectives were 1) to quantify the accuracy and uncertainty in Q_{bLS} in an ideal setting, 2) to probe the conditions under which a dispersion model based on MOST performs poorly, and 3) to validate an experimental system (i.e., source, sensors, bLS model) for examining the robustness of a bLS estimate in nonideal conditions.

[2] We neglect the impact of a plant canopy, assuming that the detector is far above vegetation and at a distance from the source that far exceeds the canopy depth. Then the effect of the canopy flow on the ensemble of paths from source to detector is negligible (Wilson et al. 2001a).

[3] In principle, there is no reason to restrict the inverse-dispersion method to ideal surface-layer problems. The capability to predict $(C/Q)_{\mathrm{sim}}$ in nonideal settings is a potential advantage of the method. However, it requires a much more complicated treatment of dispersion.

2. The bLS dispersion model

Success of the inverse-dispersion method depends upon an accurate dispersion model. To be broadly useful the model should also be flexible and easy to use. Backward Lagrangian stochastic models fit this role when looking at surface area sources. They have the proven accuracy of forward models, with added simplicity and flexibility.

a. Forward LS models

A forward Lagrangian stochastic (LS) model mimics the trajectories of thousands of tracer ''particles'' as they travel downwind of a source, and it is the most natural means of modeling dispersion in the atmospheric boundary layer (Wilson and Sawford 1996). Each trajectory is the summation of discrete changes in particle position $\Delta x_i(x_1, x_2, x_3 = x, y, z$: the along-wind, crosswind, and vertical coordinates) and velocity $\Delta u_i(u_1, u_2, u_3 = u, v, w$: the along-wind, crosswind, and vertical velocities) over time steps Δt, according to the algorithm

$$\Delta u_i = a_i \Delta t + b_i R_i \quad \text{and} \quad \Delta x_i = u_i \Delta t. \tag{2}$$

The coefficients a_i and b_i of the ''Langevin equation'' are functions of position and velocity, and R_i is a Gaussian random number (from a population having zero average and variance Δt).

The correct form of a_i and b_i is an ongoing research problem—as yet, there is no uniquely correct solution for multidimensional models. A solution given by Thomson (1987) for ''Gaussian turbulence'' (i.e., velocity probability density functions are Gaussian) is a common choice for the surface layer. It requires specification of the average Eulerian velocity in each direction (U, V, and W), the corresponding velocity variances (σ_u^2, σ_v^2, and σ_w^2), the velocity fluctuation covariances ($\langle u'v' \rangle$, $\langle u'w' \rangle$, $\langle v'w' \rangle$), and the turbulent kinetic energy dissipation rate (ε). In the ideal surface layer, we will assume a stationary atmosphere with an average vertical velocity $W = 0$ and, because the y coordinate is perpendicular to the average wind direction, we take $V = \langle u'v' \rangle = \langle v'w' \rangle = 0$ and $\langle u'w' \rangle = -u_*^2$. With u_*, σ_u^2, and σ_v^2 constant with height, but allowing σ_w^2 to be height dependent, Thomson's solution reduces to

$$\begin{aligned}
a_u &= -\frac{1}{2(\sigma_u^2\sigma_w^2 - u_*^4)} b_u^2[\sigma_w^2(u - U) + u_*^2 w] + w\frac{\partial U}{\partial z},\\
a_v &= -\frac{1}{2} b_v^2 \frac{v}{\sigma_v^2},\\
a_w &= -\frac{1}{2(\sigma_u^2\sigma_w^2 - u_*^4)} b_w^2[u_*^2(u - U) + \sigma_u^2 w] + \frac{1}{2}\frac{\partial \sigma_w^2}{\partial z}\\
&\quad + \frac{1}{2(\sigma_u^2\sigma_w^2 - u_*^4)}\left[u_*^2 \frac{\partial \sigma_w^2}{\partial z}(u - U)w + \sigma_u^2 \frac{\partial \sigma_w^2}{\partial z} w^2\right];
\end{aligned} \tag{3}$$

the coefficients of the stochastic term are

$$b_u = b_v = b_w = b = \sqrt{C_0 \varepsilon}, \tag{4}$$

where C_0 is a ''universal'' constant (reported values range between 2 and 9).

b. Backward LS model

In a bLS model the *upwind* trajectories of particles are calculated from M (Fig. 1). To this end, only a slight modification of the above forward Langevin model is needed (Flesch et al. 1995): the time increment Δt will be negative, and there is a sign reversal on the first term on the right-hand side of each a coefficient (the ''damping'' terms). The important information from the backward trajectories is the set of ''touchdown'' locations (x_0, y_0) where particles impact the ground,[4] and vertical ''touchdown velocities'' at impact w_0. With these, $(C/Q)_{\text{sim}}$ is calculated as

$$(C/Q)_{\text{sim}} = \frac{1}{N} \sum \left| \frac{2}{w_0} \right|, \tag{5}$$

where N is the total number of (computational) particles released from M and the summation covers only touchdowns within the source. An important advantage of backward models is the ease with which complex source shapes can be handled.

c. Using a line-average concentration

In our experiment a line-average concentration (C_L), measured by an open-path laser aligned parallel to the ground (section 3c), is the basis for Q inference. This approach requires a slight modification to the procedure described above for a point sensor. We simulate C_L as the average of P point concentrations equispaced along the laser path. An ensemble of backward trajectories is calculated from each of these points, and

$$(C_L/Q)_{\text{sim}} = \frac{1}{P} \sum_{j=1}^{P} \left(\frac{1}{N} \sum \left| \frac{2}{w_0} \right| \right), \tag{6}$$

where N is the number of particles released from each point and the inner summation refers only to touchdowns within the source. The Q_{bLS} is found by dividing $(C_L - C_b)$ by this $(C_L/Q)_{\text{sim}}$.

Using a line-averaging sensor has the potential to reduce error in the inverse-dispersion method. Consider a laser positioned downwind of a tracer source. Assume that the laser path is perpendicular to the mean wind (parallel to the y axis) and completely traverses the plume by a large margin. Then, the laser signal C_L is indifferent to the y coordinates of gas parcels that lie within the beam, and $(C_L/Q)_{\text{sim}}$ is insensitive to modeled lateral displacement. This insensitivity is an important

[4] The LS models do not resolve the atmosphere below a height z_r representing ''ground.'' When a particle crosses z_r (touchdown), it is ''reflected'' back into the resolved atmosphere.

consideration because modeling horizontal dispersion is more difficult (less skillful) than modeling vertical dispersion, owing to the unpredictable ''slow'' turbulent scales of motion in u and v.

d. Application details

In the bLS model we must specify a handful of wind statistics (U, σ_u, σ_v, σ_w, and ε) for the surface layer. We use traditional MOST-based formulas for these statistics, based on u_*, L, and z_0, as detailed in the appendix.

In each simulation $N = 25\,000$ particles are released from a sensor location (x_m, y_m, z_m) with random velocities consistent with the wind statistics at z_m. Each particle is followed 500 m upwind (beyond the range of interest) and abandoned. When calculating $(C_L/Q)_{\mathrm{sim}}$, we use $P = 50$ points to represent a line average. With horizontal homogeneity we do not need to recalculate trajectories for each P location but instead repeatedly translate a single set of touchdown points to each location.

The time step Δt in the Langevin equations should be a fraction of the velocity decorrelation time scale for a particle (the Lagrangian time scale τ_L). This scale varies with position and the turbulent state of the atmosphere. Following tradition, we specify (Rodean 1996)

$$\tau_L = \frac{2\sigma_w^2}{b^2} = \frac{2\sigma_w^2}{C_0\varepsilon} \tag{7}$$

(where b is the Langevin coefficient) and set $\Delta t = 0.02\tau_L$.

The roughness length z_0 is taken as the lower model boundary. When a particle crosses z_0 it is ''bounced'' and the sign of the along-wind and vertical velocity fluctuations [$(u - U)$ and w] are reversed to retain proper u–w correlation. The horizontal position and vertical velocity at each of these touchdowns are recorded.

3. Field experiment

a. Ellerslie site

Our gas release experiment took place during 6 days in May and June of 2001, near Ellerslie, Alberta, Canada, in a large alfalfa–clover field (Fig. 2). Initially, the field was short stubble (height was approximately 5 cm), but by the end of the experiment there was a sparse vegetation cover that was 15–20 cm tall (because of drought).

From a meteorological perspective, the site was nearly ideal. The minimum upwind ''fetch'' of uniform land away from our tracer source was 200 m, where the ''break'' was merely a barbed-wire fence bounding another field of similar character. The nearest significant change in land cover lay more than 500 m from our source. Dates, times, and general meteorological conditions during gas releases are given in Table 1.

b. Tracer source

A synthetic source was created to approximate a 6 m × 6 m square area source (see Fig. 2). One-inch-diameter (2.54 cm) polyvinyl chloride (PVC) pipe was used to construct a manifold having 36 outlets on a square grid. Outlets were drilled into the pipe with a 0.5-mm-diameter bit. A gas cylinder was coupled to the manifold through a regulator and flowmeter (rotameter).

Our tracer gas was CH_4 released from high pressure cylinders (99.1% purity) at flow rates between 15 and 50 L min^{-1}.[5] Each release lasted from 1 to 3 h. The cylinder valve was manually adjusted to maintain a nominally constant flow rate, with adjustment occurring every minute or two as necessary. We estimate a 10% uncertainty in Q due to flow-rate fluctuations, observer error in reading the rotameter scale, and gas temperature variability inside the rotameter (which affects calibration).

An even release of gas across the source requires the 36 outlet perforations to be identical (we *assume* that this is the case) and the head loss across each outlet to be much greater than the head loss around the manifold piping. We calculated a head loss across one leg of the manifold pipe (assuming laminar flow) and across each outlet (assuming a ''reentrant'' outlet shape) and found that the loss across the outlet is about 1000 times that through the manifold.

c. Methane concentration measurements

1) Methane laser

Methane was measured using two open-path lasers (GasFinder, Boreal Laser, Inc., Edmonton, Alberta, Canada.)[6] A collimated beam from a tunable infrared laser diode is aimed at a distant compound mirror (retroreflector) whence it is reflected back to the receiver optics and a detector. The returning power is proportional to the methane concentration between the laser and the retroreflector (i.e., C_L). The C_L is calculated from the ratio of the external absorption to an internal reference-cell absorption and is immune to uncontrollable factors such as wind-induced sway of the laser and retroreflector, degradation of lenses, and so forth.

Calibration of the lasers was adjusted retrospectively. Background methane (C_b) was periodically measured

[5] As a test of accuracy, we calculated total methane in two cylinders via the rotameter (from recorded release rates and release times), which gave 5.06 and 5.12 kg. The manufacturer reports the mass at 4.99 kg.

[6] Listing of source or everyday names is for the information of the reader and does not imply endorsement or preferential treatment by the University of Alberta or the U.S. Department of Agriculture.

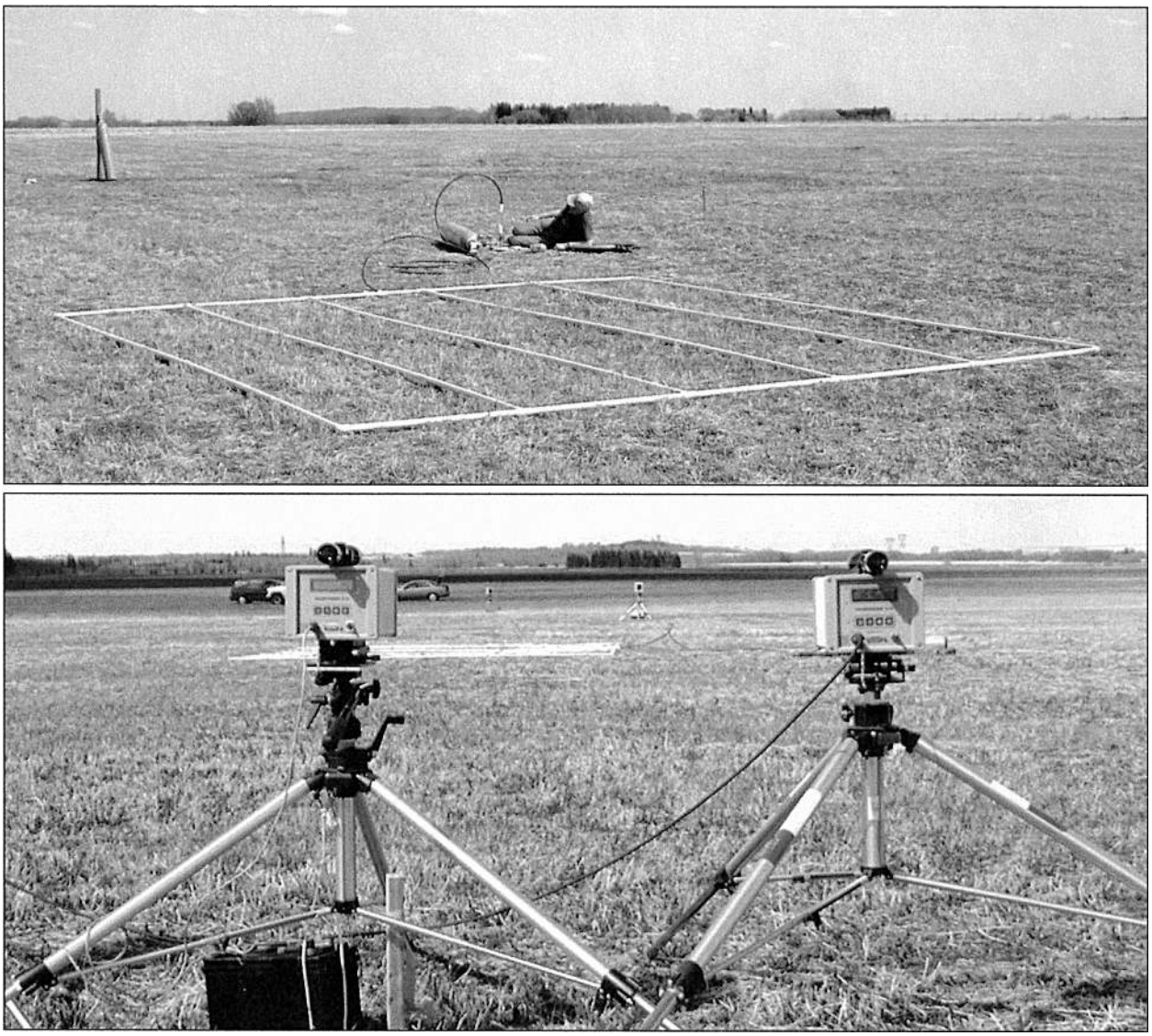

FIG. 2. The experimental site: (top) the synthetic tracer source and (bottom) two laser receivers in the foreground with retroreflectors in the background (the tracer source is also visible).

with the lasers during 16 days in May and June. Ratiometric calibration factors were introduced so that each laser gave C_b = 1.95 ppm when averaged over these observations. This was the average background for the Edmonton region during the experiment, as routinely measured by the provincial government of Alberta. This recalibration was done according to the manufacturer's instructions.

The laser units recorded C_L every minute. These readings were averaged into 15-, 30-, or 120-min values. To convert mixing ratio concentrations (ppm) to absolute concentration (g m^{-3}) we used the measured air temperature for each observation period and assumed an ambient atmospheric pressure of 930 hPa.

2) LASER POSITIONS

During the experiment the two laser units were placed in different positions around the area source. There were seven gas release periods, with two lasers operating in each period (except in one trial for which a laser was unusable), giving 13 experimental trials. Eleven different laser paths were used (some positions were used more than once) with pathlengths from 17 to 201 m (Fig. 3). The laser and retroreflector were set 0.8–1.0 m above ground. Over longer pathlengths, the curvature in terrain meant that the laser-path height above ground varied slightly along the path. We took the average of the path center height and the laser/reflector height as z_m in the bLS simulations.

TABLE 1. Gas release observations. Laser and reflector positions for each trial are referenced to the (x, y) corners of the 6 m × 6 m source at (−0.5, 0.5), (5.5, 0.7), (−0.3, −5.5), (5.7, −5.3), where x and y are the east–west and north–south coordinates (m), respectively. The sonic anemometer–derived friction velocity u_*, Obukhov length L, roughness length z_0, and average wind direction β are given. The average wind speed S, along-wind velocity U, and turbulent fluctuations $\sigma_{u,v,w}/u_*$ are given for height z_{son}. Measured methane concentration C_L, the assumed background concentration C_b, and emission rate Q are also given.

Time (LST)	S (m s^{-1})	U (m s^{-1})	β (°)	u_* (m s^{-1})	L (m)	z_0 (m)	σ_w/u_*	σ_u/u_*	σ_v/u_*	Q (g m^{-2} s^{-1})	C_L (ppm)	C_b (ppm)
TA3-5, day 129, sonic height z_{son} = 2.0 m, avg T = 12°C, laser/reflector positions (x, y, z_m): −19, −50, 0.95 m/45, 27.5, 0.95 m												
1445	5.24	5.02	279	0.37	−13.1	5.9×10^{-3}	1.26	5.63	3.79	0.0095	2.65	1.95
1500	6.66	6.33	266	0.45	−19.6	5.3×10^{-3}	1.18	4.06	4.49	0.0095	2.62	1.96
1515	5.20	5.03	258	0.32	−10.1	2.3×10^{-3}	1.31	4.34	4.26	0.0095	2.84	1.96
1530	5.32	5.13	272	0.28	−6.3	7.0×10^{-4}	1.52	5.48	4.98	0.0095	2.72	1.97
1545	5.10	4.89	268	0.29	−19.8	1.8×10^{-3}	1.41	5.34	4.90	0.0095	2.84	1.98
1600	3.80	3.65	311	0.25	−19.0	4.3×10^{-3}	1.30	3.31	4.24	0.0095	2.84	1.98
1615	4.68	4.20	273	0.26	−5.8	1.6×10^{-3}	1.60	7.30	7.96	0.0095	2.75	1.99
1630	5.10	4.57	270	0.27	−8.4	1.4×10^{-3}	1.50	6.09	7.97	0.0095	2.76	2.00
TA3-6, day 129, sonic height z_{son} = 2.0 m, avg T = 12°C, laser/reflector positions (x, y, z_m): −61, −110, 0.85 m/95, 88, 0.85 m												
1445	5.24	5.02	279	0.37	−13.1	5.9×10^{-3}	1.26	5.63	3.79	0.0095	2.20	2.12
1500	6.66	6.33	266	0.45	−19.6	5.3×10^{-3}	1.18	4.06	4.49	0.0095	2.21	2.13
1515	5.20	5.03	258	0.32	−10.1	2.3×10^{-3}	1.31	4.34	4.26	0.0095	2.22	2.14
1530	5.32	5.13	272	0.28	−6.3	7.0×10^{-4}	1.52	5.48	4.98	0.0095	2.21	2.15
1545	5.10	4.89	268	0.29	−19.8	1.8×10^{-3}	1.41	5.34	4.90	0.0095	2.26	2.17
1600	3.80	3.65	311	0.25	−19.0	4.3×10^{-3}	1.30	3.31	4.24	0.0095	2.26	2.18
1615	4.68	4.20	273	0.26	−5.8	1.6×10^{-3}	1.60	7.30	7.96	0.0095	2.28	2.19
1630	5.10	4.57	270	0.27	−8.4	1.4×10^{-3}	1.50	6.09	7.97	0.0095	2.33	2.20
TA4-5, day 130, sonic height z_{son} = 2.0 m, avg T = 13°C, laser/reflector positions (x, y, z_m): −3.8, −8.3, 0.8 m/9.6, 2.8, 0.8 m												
1615	3.54	3.26	295	0.23	−7.9	4.0×10^{-3}	1.42	5.70	5.76	0.0047	2.36	2.00
1630	4.07	3.68	263	0.29	−11.8	8.1×10^{-3}	1.28	4.43	6.03	0.0047	3.53	1.99
1645	3.29	3.13	277	0.08	−0.2	3.5×10^{-8}	4.20	19.99	11.40	0.0047	3.78	1.98
1700	3.27	3.04	272	0.18	−2.3	7.9×10^{-4}	1.97	7.88	6.60	0.0047	2.97	1.98
1715	3.14	2.91	273	0.14	−2.2	1.7×10^{-4}	2.08	6.48	8.75	0.0047	3.03	1.97
1730	3.63	3.36	307	0.27	−11.2	8.9×10^{-3}	1.21	4.75	5.11	0.0047	2.28	1.96
1745	1.24	0.88	71	0.06	−0.5	5.5×10^{-4}	3.19	12.47	14.37	0.0094	11.80	1.96
1800	3.11	2.99	299	0.20	−14.2	3.5×10^{-3}	1.29	5.94	4.16	0.0094	2.65	1.95
TA4-6, day 130, sonic height z_{son} = 2.0 m, avg T = 13°C, laser/reflector positions (x, y, z_m): −32, −32.5, 0.95 m/58, 8.9, 0.95 m												
1615	3.54	3.26	295	0.23	−7.9	4.0×10^{-3}	1.42	5.70	5.76	0.0047	2.90	2.30
1630	4.07	3.68	263	0.29	−11.8	8.1×10^{-3}	1.28	4.43	6.03	0.0047	2.67	2.30
1645	3.29	3.13	277	0.08	−0.2	3.5×10^{-8}	4.20	19.99	11.40	0.0047	2.96	2.30
1700	3.27	3.04	272	0.18	−2.3	7.9×10^{-4}	1.97	7.88	6.60	0.0047	2.89	2.30
1715	3.14	2.91	273	0.14	−2.2	1.7×10^{-4}	2.08	6.48	8.75	0.0047	2.98	2.30
1730	3.63	3.36	307	0.27	−11.2	8.9×10^{-3}	1.21	4.75	5.11	0.0047	2.90	2.30
1745	1.24	0.88	71	0.06	−0.5	5.5×10^{-4}	3.19	12.47	14.37	0.0094	2.71	2.30
1800	3.11	2.99	299	0.20	−14.2	3.5×10^{-3}	1.29	5.94	4.16	0.0094	3.57	2.30
TA5-5, day 131, sonic height z_{son} = 2.0 m, avg T = 16°C, laser/reflector positions (x, y, z_m): 5.0, −27.9, 0.95 m/6.9, 22.4, 0.95 m												
1545	2.59	1.92	245	0.27	−8.7	6.9×10^{-2}	1.30	5.93	5.61	0.0094	3.39	1.94
1600	2.40	2.20	207	0.23	−8.8	2.6×10^{-2}	1.17	4.83	4.20	0.0094	5.01	1.94
1615	3.72	3.22	231	0.22	−4.1	2.6×10^{-3}	1.79	7.02	8.15	0.0094	3.06	1.93
1630	3.93	3.59	238	0.27	−8.5	5.8×10^{-3}	1.34	3.67	5.79	0.0094	2.50	1.92
1645	2.46	1.53	299	0.09	−0.5	3.0×10^{-4}	3.18	12.93	22.06	0.0094	3.81	1.92
1700	3.17	2.59	253	0.11	−0.7	3.0×10^{-5}	2.94	8.80	16.05	0.0141	3.38	1.91
1715	2.38	1.64	236	0.17	−2.7	1.6×10^{-2}	1.83	8.39	9.82	0.0141	4.43	1.90
1730	3.59	3.39	284	0.24	−6.7	3.8×10^{-3}	1.37	5.36	5.06	0.0141	2.90	1.90
TA5-6, day 131, sonic height z_{son} = 2.0 m, avg T = 16°C, laser/reflector positions (x, y, z_m): 29.1, −54.8, 0.90 m/1.4, 44.5, 0.90 m												
1545	2.59	1.92	245	0.27	−8.7	6.9×10^{-2}	1.30	5.93	5.61	0.0094	2.63	1.64
1600	2.40	2.20	207	0.23	−8.8	2.6×10^{-2}	1.17	4.83	4.20	0.0094	2.91	1.66
1615	3.72	3.22	231	0.22	−4.1	2.6×10^{-3}	1.79	7.02	8.15	0.0094	2.75	1.69
1630	3.93	3.59	238	0.27	−8.5	5.8×10^{-3}	1.34	3.67	5.79	0.0094	2.65	1.71
1645	2.46	1.53	299	0.09	−0.5	3.0×10^{-4}	3.18	12.93	22.06	0.0094	2.35	1.73
1700	3.17	2.59	253	0.11	−0.7	3.0×10^{-5}	2.94	8.80	16.05	0.0141	3.50	1.75
1715	2.38	1.64	236	0.17	−2.7	1.6×10^{-2}	1.83	8.39	9.82	0.0141	3.01	1.77
1730	3.59	3.39	284	0.24	−6.7	3.8×10^{-3}	1.37	5.36	5.06	0.0141	3.32	1.79
A1-5, day 164, sonic height z_{son} = 2.1 m, avg T = 15°C, laser/reflector positions (x, y, z_m): 5.0, −27.9, 0.95 m/6.9, 22.4, 0.95 m												
1115	2.65	2.20	267	0.10	−0.6	5.0×10^{-5}	2.96	11.77	12.39	0.0086	4.39	1.85
1130	3.00	2.85	285	0.28	−12.6	2.4×10^{-2}	1.16	3.64	3.23	0.0086	3.00	1.85
1145	2.00	1.64	281	0.17	−2.0	1.4×10^{-2}	1.82	8.24	5.92	0.0086	5.38	1.85
1200	3.05	2.62	312	0.29	−11.7	3.7×10^{-2}	1.14	2.83	5.30	0.0086	4.33	1.85

TABLE 1. (*Continued*)

Time (LST)	S (m s^{-1})	U (m s^{-1})	β (°)	u_* (m s^{-1})	L (m)	z_0 (m)	σ_w/u_*	σ_u/u_*	σ_v/u_*	Q (g m^{-2} s^{-1})	C_L (ppm)	C_b (ppm)
1245	2.30	2.22	334	0.22	−1000.0	3.7×10^{-2}	1.12	2.58	2.76	0.0128	9.43	1.85
1300	1.35	0.84	290	0.11	−1.5	2.7×10^{-2}	2.32	7.46	9.65	0.0128	9.47	1.85
1315	3.28	3.21	336	0.27	−88.5	1.7×10^{-2}	1.23	3.57	2.48	0.0128	7.24	1.85
1330	2.70	2.27	325	0.21	−4.2	1.3×10^{-2}	1.63	4.53	6.67	0.0128	6.42	1.85
A2-5, day 166, sonic height z_{son} = 2.1 m, avg T = 10°C, laser/reflector positions (x, y, z_m): 5.0, −27.9, 0.95 m/6.9, 22.4, 0.95 m												
715	3.43	3.36	323	0.33	−407.7	3.5×10^{-2}	1.09	2.29	2.03	0.0090	3.95	1.97
730	3.84	3.76	318	0.32	−276.5	1.9×10^{-2}	1.16	2.68	2.38	0.0090	3.73	1.96
745	3.54	3.47	322	0.31	−126.9	2.3×10^{-2}	1.08	2.53	2.30	0.0090	4.34	1.96
800	4.00	3.92	327	0.34	−76.7	1.9×10^{-2}	1.16	2.63	2.35	0.0090	4.25	1.95
A2-6, day 166, sonic height z_{son} = 2.1 m, avg T = 7°C, laser/reflector positions (x, y, z_m): −21.5, −134.3, 0.85 m/96.5, 21.8, 0.85 m												
515	1.79	1.74	317	0.16	42.0	3.4×10^{-2}	1.20	2.66	2.52	0.0090	2.41	1.95
530	2.04	2.01	312	0.16	72.3	1.6×10^{-2}	1.24	2.83	2.02	0.0090	2.32	1.94
545	2.18	2.15	322	0.18	113.1	1.9×10^{-2}	1.16	2.66	1.97	0.0090	2.31	1.92
600	2.39	2.36	319	0.20	139.4	2.0×10^{-2}	1.18	3.10	2.05	0.0090	2.22	1.91
615	2.53	2.48	326	0.20	188.6	1.6×10^{-2}	1.25	2.78	2.62	0.0090	2.12	1.89
630	2.55	2.50	326	0.23	137.3	2.9×10^{-2}	1.21	2.65	2.18	0.0090	2.13	1.88
715	3.43	3.36	323	0.33	−407.7	3.5×10^{-2}	1.09	2.29	2.03	0.0090	2.07	1.87
730	3.84	3.76	318	0.32	−276.5	1.9×10^{-2}	1.16	2.68	2.38	0.0090	2.04	1.87
745	3.54	3.47	322	0.31	−126.9	2.3×10^{-2}	1.08	2.53	2.30	0.0090	2.05	1.86
800	4.00	3.92	327	0.34	−76.7	1.9×10^{-2}	1.16	2.63	2.35	0.0090	2.02	1.86
A3-5, day 171, sonic height z_{son} = 2.1 m, avg T = 9°C, laser/reflector positions (x, y, z_m): −17.1, 0.0, 1.0 m/16.4, −0.1, 1.0 m												
445	1.52	1.51	129	0.08	4.0	1.3×10^{-2}	1.26	2.86	2.16	0.0087	9.62	1.94
500	2.02	2.01	123	0.11	8.5	4.5×10^{-3}	1.23	2.82	2.22	0.0087	11.29	1.96
515	2.19	2.18	135	0.15	17.4	1.1×10^{-2}	1.19	2.24	1.77	0.0087	6.99	1.97
530	2.24	2.23	128	0.14	15.4	6.7×10^{-3}	1.26	2.20	1.66	0.0087	8.29	1.98
545	2.40	2.38	129	0.17	28.3	1.1×10^{-2}	1.19	2.15	1.65	0.0087	7.41	2.00
600	2.45	2.42	128	0.18	30.7	1.3×10^{-2}	1.28	2.40	1.94	0.0087	7.53	2.01
615	2.51	2.48	152	0.21	42.2	2.4×10^{-2}	1.19	3.16	1.95	0.0087	5.36	2.02
630	2.63	2.60	145	0.22	100.0	2.0×10^{-2}	1.19	2.44	1.68	0.0087	5.12	2.03
645	2.16	2.12	146	0.22	110.1	4.8×10^{-2}	1.16	2.37	1.83	0.0087	6.34	2.05
700	2.49	2.45	156	0.23	418.5	3.1×10^{-2}	1.16	2.52	2.00	0.0087	6.91	2.06
A3-6, day 171, sonic height z_{son} = 2.1 m, avg T = 9°C, laser/reflector positions (x, y, z_m): −103, 16.1, 1.0 m/96.5, 21.8, 1.0 m												
515	2.19	2.18	135	0.15	17.4	1.1×10^{-2}	1.19	2.24	1.77	0.0087	2.85	1.92
530	2.24	2.23	128	0.14	15.4	6.7×10^{-3}	1.26	2.20	1.66	0.0087	2.89	1.92
545	2.40	2.38	129	0.17	28.3	1.1×10^{-2}	1.19	2.15	1.65	0.0087	2.72	1.92
600	2.45	2.42	128	0.18	30.7	1.3×10^{-2}	1.28	2.40	1.94	0.0087	2.63	1.92
615	2.51	2.48	152	0.21	42.2	2.4×10^{-2}	1.19	3.16	1.95	0.0087	2.63	1.92
630	2.63	2.60	145	0.22	100.0	2.0×10^{-2}	1.19	2.44	1.68	0.0087	2.51	1.92
645	2.16	2.12	146	0.22	110.1	4.8×10^{-2}	1.16	2.37	1.83	0.0087	2.61	1.92
700	2.49	2.45	156	0.23	418.5	3.1×10^{-2}	1.16	2.52	2.00	0.0087	2.57	1.92
A4-5, day 172, sonic height z_{son} = 2.1 m, avg T = 10°C, laser/reflector positions (x, y, z_m): −32.0, 9.5, 1.0 m/57.8, 8.9, 1.0 m												
430	1.82	1.79	189	0.06	3.1	2.1×10^{-4}	1.39	4.99	5.31	0.0087	5.76	2.03
445	1.71	1.69	186	0.07	3.1	2.1×10^{-3}	1.43	3.10	2.86	0.0087	5.90	2.03
515	1.46	1.45	212	0.07	2.6	2.5×10^{-2}	1.55	5.53	3.11	0.0087	6.81	2.03
530	0.71	0.66	226	0.02	−8.3	8.4×10^{-7}	1.96	5.76	3.24	0.0087	5.93	2.03
545	1.14	1.10	213	0.05	5.2	1.2×10^{-3}	1.22	7.02	3.26	0.0087	5.49	2.03
600	1.31	1.28	195	0.06	2.9	9.5×10^{-3}	1.35	3.64	4.80	0.0087	7.05	2.03
615	0.90	0.88	221	0.09	21.4	3.7×10^{-2}	1.03	5.01	3.09	0.0087	9.13	2.03
630	0.56	0.52	247	0.02	4.4	5.0×10^{-5}	3.40	7.17	6.17	0.0087	5.83	2.03
645	0.38	0.37	228	0.01	0.1	5.6×10^{-10}	5.61	7.82	4.82	0.0087	7.38	2.03
700	0.88	0.85	236	0.09	−11.8	1.2×10^{-2}	1.26	2.78	2.47	0.0087	6.76	2.03
A4-6, day 172, sonic height z_{son} = 2.1 m, avg T = 10°C, laser/reflector positions (x, y, z_m): −116, 60.1, 1.0 m/97.6, 53.0, 1.0 m												
430	1.82	1.79	189	0.06	3.1	2.1×10^{-4}	1.39	4.99	5.31	0.0087	3.41	2.07
445	1.71	1.69	186	0.07	3.1	2.1×10^{-3}	1.43	3.10	2.86	0.0087	3.07	2.07
515	1.46	1.45	212	0.07	2.6	2.5×10^{-2}	1.55	5.53	3.11	0.0087	3.44	2.07
530	0.71	0.66	226	0.02	−8.3	8.4×10^{-7}	1.96	5.76	3.24	0.0087	4.26	2.07
545	1.14	1.10	213	0.05	5.2	1.2×10^{-3}	1.22	7.02	3.26	0.0087	4.35	2.07
600	1.31	1.28	195	0.06	2.9	9.5×10^{-3}	1.35	3.64	4.80	0.0087	3.42	2.07
615	0.90	0.88	221	0.09	21.4	3.7×10^{-2}	1.03	5.01	3.09	0.0087	3.56	2.07
630	0.56	0.52	247	0.02	4.4	5.0×10^{-5}	3.40	7.17	6.17	0.0087	2.89	2.07
645	0.38	0.37	228	0.01	0.1	5.6×10^{-10}	5.61	7.82	4.82	0.0087	2.91	2.07
700	0.88	0.85	236	0.09	−11.8	1.2×10^{-2}	1.26	2.78	2.47	0.0087	2.68	2.07

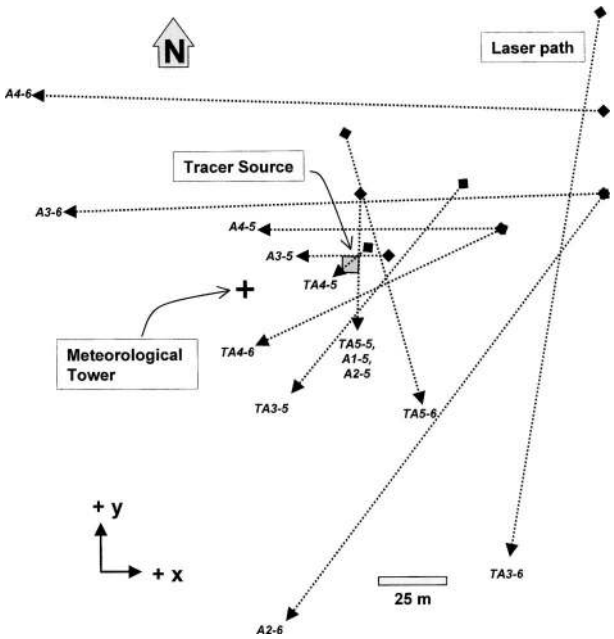

FIG. 3. Map of the 11 laser paths used in the experiment. The experiment associated with each path is given adjacent to the arrow. The tracer source is shown by the shaded square.

3) BACKGROUND CONCENTRATION

The lasers were adjusted to give an average C_b of 1.95 ppm over the experiment, but there was C_b variation over time (from 1.6 to 2.3 ppm during our trials). The C_b from each laser was measured before and after each gas release. Often, there was a difference between the two, sometimes significantly so (e.g., 1.65 vs 1.80 ppm). We treated C_b as trending linearly with time during a release. Section 4a(3) describes how this assumption can affect Q inference.

d. Meteorological observations

Two alternative approaches were used to give u_*, z_0, L, and β for the bLS model: sonic anemometer observations and a profile system.

1) SONIC ANEMOMETER MEASUREMENTS

A three-dimensional sonic anemometer (CSAT-3, Campbell Scientific, Inc., Logan, Utah) was placed on a tower at height $z_{son} \approx 2$ m above ground (the height varied slightly during the experiment). Wind velocity and temperature were sampled at a frequency of 16 Hz. The sonic anemometer was reoriented and repositioned as necessary to ensure frontal approach flow and to avoid the wake of the tower. We calculated wind direction with respect to a north–south coordinate system constructed with a global positioning system (GPS):

$$\beta = \tan^{-1}\left(-\frac{V_{raw}}{U_{raw}}\right) + \beta_{offset}, \tag{8}$$

where U_{raw} and V_{raw} are the average horizontal velocities with respect to the sonic anemometer housing and β_{offset} is the angular offset of the housing with respect to our coordinate system. Raw velocity and heat flux statistics were transformed into along-/crosswind coordinates, using a sequence of two coordinate rotations (Kaimal and Finnigan 1994): first setting the average crosswind velocity $V = 0$ (yaw correction) and then setting the average vertical velocity $W = 0$ (pitch correction). Separate corrections were done for each observation period. From these transformed velocities, we calculated the mean along-wind velocity U_{son}, the friction velocity

$$u_{*son} = \sqrt[4]{\langle u'w'\rangle^2 + \langle v'w'\rangle^2}, \tag{9}$$

and the Obukhov length

$$L_{son} = -\frac{u_{*son}^3 T}{k_v g \langle w'T'\rangle} \tag{10}$$

(where T is the mean absolute air temperature, k_v is the von Kármán constant, and g is the gravitational acceleration).[7] The roughness length was chosen to reconcile the diabatically corrected log wind profile with U_{son}, u_{*son}, and L_{son}:

$$z_{0son} = \frac{z_{son}}{\exp(U_{son}k_v/u_{*son} - \psi_{son})} \tag{11}$$

(ψ_{son} is calculated with the formulas given in the appendix). The sonic anemometer observations also provided the velocity standard deviations ($\sigma_{u,v,w}$).

2) PROFILE MEASUREMENTS

Alternatives to the sonic anemometer–derived u_*, z_0, and L were calculated by analyzing vertical profiles of average cup wind speed S and temperature T. A 6-m tower was instrumented with five cup anemometers (Model 011-4, Climet Instruments Co.) at heights z = 0.65, 1.12, 2.12, 3.6, and 6.05 m and two shielded and ventilated thermocouple pairs that measured temperature differences between z = 0.29–1.35 m and z = 1.35–5.75 m. Comparisons between the cup and sonic S showed cup overspeeding of 8%, with no systematic trend with turbulence level. We accordingly adjusted all cup wind speeds by 8%. To avoid periods for which the cups may have stalled, we ignored observations of S of less than 1 m s^{-1}.

We deduced u_{*pro} and L_{pro} as those values giving theoretical MOST profiles of S and T that best fit the measurements. The procedure of Argete and Wilson (1989) was used, presupposing the von Kármán constant k_v = 0.4 and assigning the uncertainty factors that normalize the fitting errors as $g_S = \max[0.02, 0.01S(6.05\text{ m})]$ m

[7] "Acoustic" temperature from the sonic anemometer was used for T. We used this rather than the proper virtual temperature when calculating L_{son}. Because the surface was dry, this error should be small (see Garratt 1992).

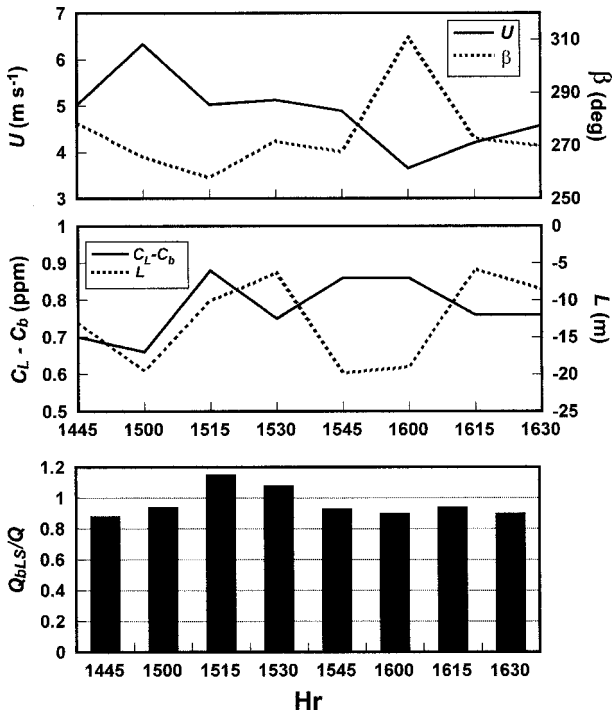

FIG. 4. Observations from trial TA3-5. (top) Average alongwind velocity U (at $z_{son} = 2$ m) and average wind direction β. (middle) Average methane concentration rise above background $C_L - C_b$ and the Obukhov length L for 15-min periods. (bottom) The bLS predictions of the source emission rate scaled on the actual emission rate Q_{bLS}/Q and plotted vs local time.

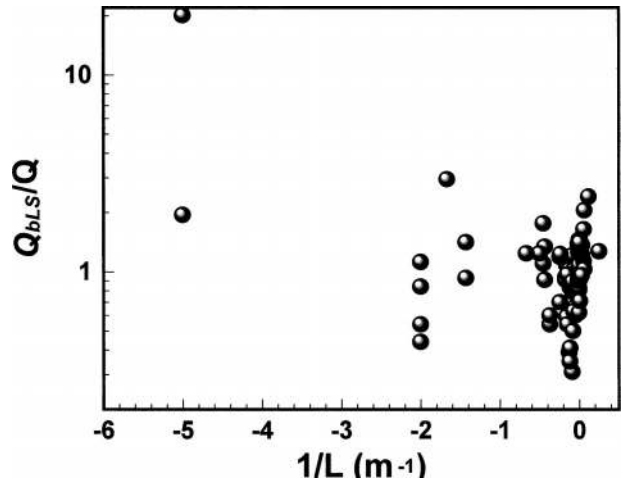

FIG. 5. Ratio of predicted to actual emission rate (Q_{bLS}/Q) vs the reciprocal of the Obukhov length ($1/L$). All observations except those from trial A4 are shown.

s^{-1} and $g_T = \max(0.1, 0.1|\Delta T_{13}|)$ °C (where $|\Delta T_{13}|$ is the magnitude of the temperature difference between $z = 0.29$ and 5.57 m). Having selected u_{*pro} and L_{pro}, we took z_{0pro} as the value required to best fit the observed S profile.

4. Emission estimates

Accurate inference of Q depends on the accuracy of our MOST-based description of the atmosphere. Although MOST profiles are seldom ''perfect,'' previous comparisons show that when a model correctly specifies U and σ_w at a reference height somewhere in the plume, and gives a *plausible* extrapolation away from that height, an ensemble of tracer trajectories will be skillful. Nevertheless, periods of rapid atmospheric change or extreme stability invalidate the very precepts of MOST and make our estimates of Q suspect. One trial period illustrates this effect. Trial A4 takes place in a light-wind, sunrise transition period, and Q_{bLS} is very inaccurate. In the discussion that follows we ignore this trial, and later we focus on it as a case study of an unsuccessful bLS application.

a. Q_{bLS} using sonic observations

Here we discuss Q_{bLS} estimates from 15-min-average laser concentrations C_L and the corresponding sonic-derived u_{*son}, z_{0son}, L_{son}, and β. Figure 4 illustrates the success of trial TA3-5, a period during which the laser path was 15–20 m downwind of the source. During this experiment U_{son} ($z = 2$ m) varies from 3.65 to 6.33 m s^{-1}, L_{son} varies from -6 to -20 m, and β varies from 258° to 311°. This variation results in time-varying C_L and C_L/Q ratios, but, as Fig. 4 shows, the bLS model integrates these changes with sufficient skill to yield a good estimate of Q. The average ratio of the bLS estimate to the actual emission rate (Q_{bLS}/Q) for this trial is 0.96, meaning that on average the bLS technique underpredicts Q by only 4%.

For all $n = 88$ observation periods (excluding A4) the Q_{bLS} estimates are not so accurate as in TA3-5. The average Q_{bLS}/Q is 1.27, meaning that, on average, the bLS technique overpredicts Q by 27% (see Fig. 5). The estimates are also characterized by large variability, with the standard deviation in Q_{bLS}/Q ($\sigma_{Q/Q}$) being 2.07. However, a handful of outliers are associated with extreme stability, and our results are much improved if we reject these periods.

1) EXCLUDING EXTREME STABILITIES

Eleven of the 88 observation periods are characterized by strong instability, with -2 m $\leq L_{son} \leq -0.2$ m. If we ignore these extremes, the average Q_{bLS}/Q falls to 1.02. Inaccuracy in periods of extreme stability is not surprising given the limitations of MOST. If we take a conservative view that the legitimacy of our MOST-based atmospheric description requires $|z/L| < 1$ (a commonly used requirement) and given our dependence on meteorological observations at $z_{son} \approx 2$ m, this suggests avoiding periods when $|L| \leq 2$ m. In the results that follow we therefore exclude those periods (unless otherwise indicated).

Figure 6 illustrates Q_{bLS}/Q across the $n = 77$ periods

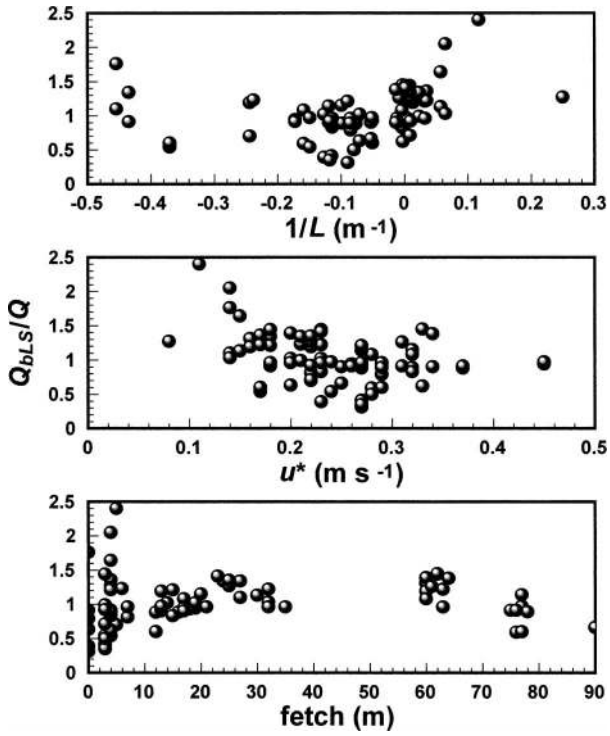

FIG. 6. Ratio of predicted to actual emission rate (Q_{bLS}/Q) vs (top) the reciprocal of the Obukhov length L, (middle) the friction velocity u_*, and (bottom) laser fetch. Periods of extreme stability ($|L| < 2$ m) and trial A4 are excluded.

of ''moderate to weak'' stratification. The Q_{bLS}/Q averages a very accurate 1.02, but the period-to-period variability is large, with $\sigma_{Q/Q} = 0.36$. The accuracy varies with stability: Q_{bLS}/Q averages 0.87 in unstable stratification ($1/L \leq -0.02$ m^{-1}), 1.12 in near-neutral stratification (-0.02 m$^{-1} < 1/L < 0.02$ m^{-1}), and 1.38 in stable cases ($1/L \geq 0.02$ m^{-1}). This trend toward decreasing accuracy as the atmosphere becomes more stable can be interpreted as a trend toward inaccuracy as u_* decreases (which is associated with stability).

2) Influence of laser–source distance

As the downwind distance between the center of the source and the laser path (fetch) decreases, variability in Q_{bLS}/Q increases (Fig. 6). In five trials the laser path was aligned either diagonally across the source (fetch = 0 m) or along the edge of the source (fetch = 3–10 m, depending on wind direction). Eliminating these short-fetch cases drops the standard deviation $\sigma_{Q/Q}$ from 0.36 to 0.22 ($n = 46$). We also find the previously noted trend toward Q_{bLS} overprediction in stable conditions is then muted, with Q_{bLS}/Q averaging 0.95 in unstable cases and 1.16 in stable cases.

Two factors may account for the increased error in Q_{bLS} with decreasing fetch. Some error is entailed in our assumption of a uniform area source, contradicting the reality of 36 distinct point sources. This difference will be more apparent at short fetches. A more fundamental problem is the possibility that at short fetches the laser path lies at the edge of the tracer plume. This carries greater uncertainty in $(C/Q)_{sim}$, because trajectories at the plume margin are by definition ''extreme,'' whereas, at present, dispersion models cannot be specifically tailored to reproduce the (unknown) statistical extremes of displacement.

After eliminating short-fetch cases, the $\sigma_{Q/Q}$ is approximately 0.2. This level of random error is probably about as small as one can reasonably hope for and is not easily surpassed by competing techniques for source estimation. It is important to realize that each short-term (15 min) prediction of $(C/Q)_{sim}$ corresponds to a hypothetical average of many tracer release trials, all made under identical conditions (this is true of any type of dispersion model). The stochastic variability that exists in any one trial is not represented, and it would be unrealistic to expect the one-time inference of Q to be much better than $\pm 20\%$. Considering uncertainty in our measured Q may be 10%, then a 20% variability in Q_{bLS}/Q is satisfactory.

3) Importance of C_b

Increasing the laser fetch should reduce dispersion modeling errors for the reasons discussed above. However, moving further from the tracer source decreases the resulting concentration rise above background. To maintain accuracy in Q_{bLS} requires increasing accuracy in both C_L and C_b. At the longer fetches of our experiment we find that Q_{bLS} becomes sensitive to assumptions about C_b.

Figure 7 shows C_L during trial TA3-6 (fetch $\sim$ 80 m). The C_b is 2.10 ppm before gas release and 2.21 ppm after. Our standard procedure is to assume a linear trend in C_b during the release, and Fig. 7 shows the resulting Q_{bLS}/Q values. What if C_b did not change linearly? Our experience is of occasional step changes in C_L correlated with changes in the laser light levels (an ancillary laser output). Figure 7 shows alternative Q_{bLS}/Q estimates assuming a step change in C_b from 2.10 to 2.20 ppm at a time of rising laser light levels. This alternative gives a surprising improvement, with the average Q_{bLS}/Q increasing from 0.83 to 0.96. There is no way to know the actual C_b trend. It is fortunate that most of our trials have a smaller fetch and much less sensitivity to the treatment of C_b.

4) Using actual turbulence

Could some of the period-to-period variability in Q_{bLS}/Q be due to the departure of wind statistics from the MOST-based formulas used in the bLS model? Could our bLS estimates be improved by using the actual wind statistics? Compare the σ_w observations during our experiment with the values calculated in our bLS model (Fig. A1). Although the model formulas re-

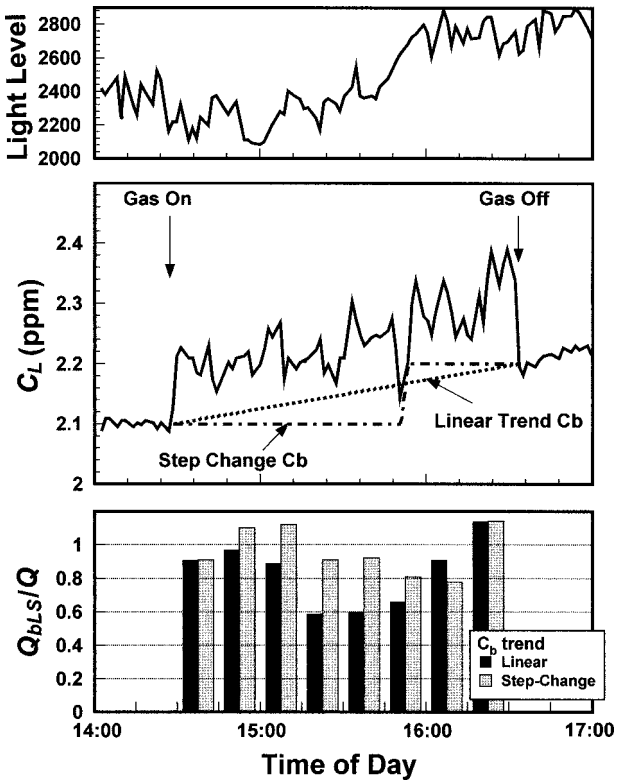

FIG. 7. (middle) The concentration record C_L for trial TA3-6 plotted vs local time. The rise in background concentration C_b during gas release is alternatively described by a linear trend and a step change [(top) the step change is correlated with a rise in laser light level]. (bottom) The ratio of predicted to actual emission rate (Q_{bLS}/Q), illustrated using both the linear and step change assumptions.

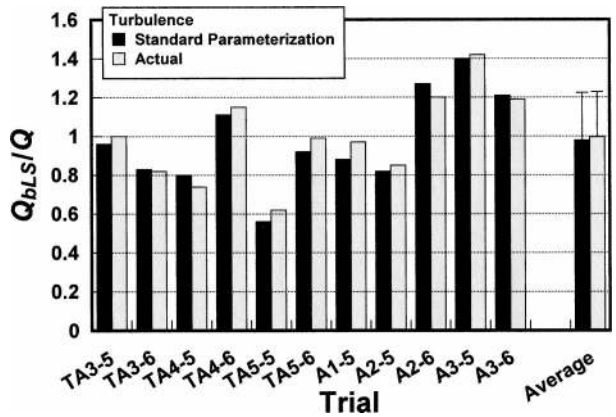

FIG. 8. Trial-average ratio of predicted to actual emission rate (Q_{bLS}/Q) using both standard parameterized turbulence statistics $\sigma_{u,v,w}$ and the actual $\sigma_{u,v,w}$. The farthest-right columns are the cross-trial average of Q_{bLS}/Q, with the error bars representing the standard deviation.

produce the average behavior of σ_w, there is scatter about the values.

We recomputed $(C_L/Q)_{\mathrm{sim}}$ after adjusting the parameters b_u, b_v, and b_w of Eqs. (A3)–(A6) to reproduce the observed σ_u, σ_v, and σ_w at z_{son}. Figure 8 shows a trial-by-trial comparison of the average Q_{bLS}/Q using standard values ($b_{u,v,w}$ = 2.5, 2.0, 1.25) and those with ''tuned'' values. Overall there is no difference between the two results. Two factors may explain the lack of improvement. First, the stochastic variability in (C/Q) that exists in any one observation is not mimicked by the bLS model no matter how accurately U, σ_u, σ_v, and so on, are known. This base uncertainty cannot be reduced. Another possibility is that when $\sigma_{u,v,w}/u_*$ differs from expectation it is because there is a broad departure in the atmospheric state away from the ideal MOST ensemble. If irregularity in $\sigma_{u,v,w}$ reflects pervasive atmospheric variability, then it is not clear whether modification of $b_{u,v,w}$ alone will produce a more accurate Q_{bLS}.

5) INFLUENCE OF AVERAGING TIME

Some source estimation problems may require long averaging times for C because of limitations in measurement techniques or because expenses dictate long-interval observations. We now consider how the averaging interval affects Q_{bLS}.

What averaging time should be used when calculating Q_{bLS}? The bLS model mimics the microscale by applying fluctuations represented by $\sigma_{u,v,w}$ at a micro–time scale τ_L. In our approach the larger scales of motion act through period-to-period changes in input u_*, L, and β. This strategy, which posits a spectral gap between the small- and larger-scale motions, works well for short averaging intervals (e.g., 15 min). As averaging interval increases, the importance of larger-scale fluctuations on dispersion *within* the interval increases. These scales of motion are not mimicked in the bLS model, nor are they represented in the standard MOST relationships incorporated in the model (which have been built from traditional 15–60-min wind statistics). Therefore, applying the model to averaging periods greatly different from 15–60 min carries a risk. There are also problems with short averaging intervals (of order 1 min). They may not capture an equilibrium state of the atmosphere, a requirement for application of MOST.

To look at the impact of averaging time we select trials TA3-5, TA3-6, A3-5, and A3-6. From 2 h of continuous data in each trial, we create alternative sets of eight 15-min periods, four 30-min periods, or one 120-min period (with corresponding $u_{*\mathrm{son}}$, L_{son}, $z_{0\mathrm{son}}$, β, and C_L). We calculate Q_{bLS} for each interval choice and combine these into 2-h-average Q_{bLS} values. In all cases, an increase in averaging time systematically changes Q_{bLS}/Q (Fig. 9). In three of the four trials there is a decrease in accuracy; in one case there is improvement. In A3-6 the 120-min interval results in a 17% larger error in Q_{bLS} as compared with 15-min intervals.

We might conclude that longer averaging intervals give worse Q_{bLS} estimates, but this conclusion is not strictly true. If we increase $b_{u,v}$ to mimic the changes in

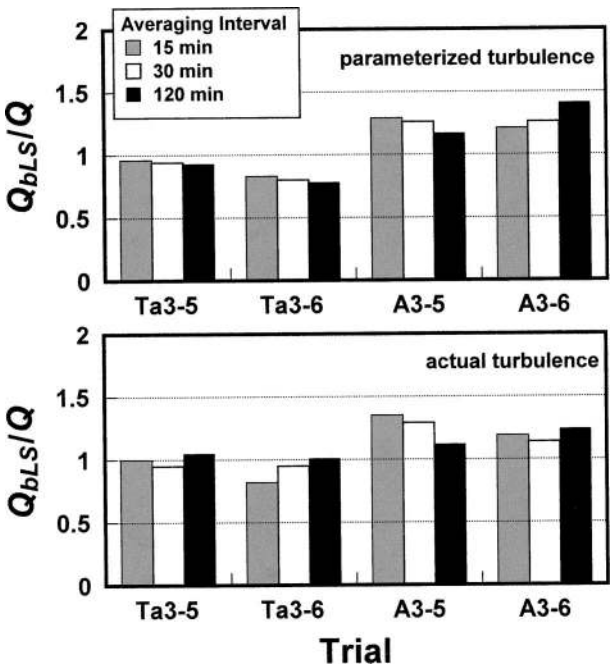

FIG. 9. Ratio of predicted to actual emission rate (Q_{bLS}/Q) for four experimental trials. Different columns are for different averaging times. (top) The predictions using standard parameterized turbulence statistics $\sigma_{u,v,w}$, and (bottom) predictions using the actual $\sigma_{u,v,w}$.

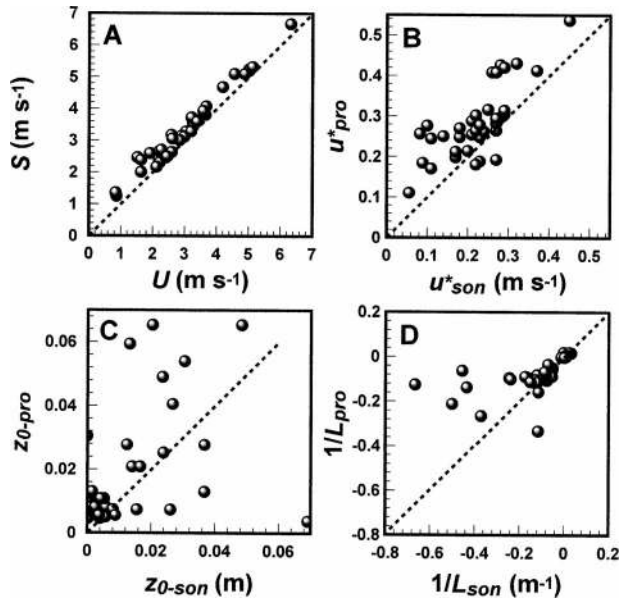

FIG. 10. A comparison of quantities measured/inferred from sonic anemometer and profile observations. (a) Differences between cup wind speed S and the along-wind velocity U measured by the sonic at $z_{\mathrm{son}} \approx 2$ m. Differences for (b) friction velocity u_*, (c) roughness length z_0, and (d) Obukhov length L (subscripts ''son'' and ''pro'' indicate a sonic anemometer or profile estimate).

$\sigma_{u,v}$ as averaging interval increases,[8] we do not see the same degradation (Fig. 9). Here, the bLS model wrongly applies the incremental increases in $\sigma_{u,v}$ to microscale turbulence and not to larger-scale fluctuations, but wrongly adding these additional fluctuations is still beneficial. This result indicates that the bLS technique can be applied to longer averaging intervals—preferably using long-interval wind statistics to drive the bLS model. However, the better choice is to use short averaging times (say 10–30 min), which maintains consistency with the traditional MOST description of the atmosphere and is true to the microscale bLS model.

b. Profile versus sonic anemometer observations

To this point we have relied on sonic anemometer estimates of u_*, L, and z_0. We now examine how profile estimates of these parameters differ from sonic anemometer estimates and the effect this has on Q_{bLS}. Consider the difference between average wind speed S and along-wind velocity U. When the turbulent intensity is low ($\sigma_{u,v} \ll U$), we can relate the two using a binomial expansion:

$$S = \overline{\sqrt{u^2 + v^2}} \simeq U\left(1 + \frac{\sigma_u^2 + \sigma_v^2}{2U^2}\right). \qquad (12)$$

In the turbulent atmosphere S always exceeds U. Our sonic anemometer observations of S/U vary from 1.01 during stable periods to 1.61 in very unstable periods (at $z_{\mathrm{son}} \approx 2$ m).

In the bLS model we want u_*, L, and z_0 that will result in an accurate profile of U and not S, because particles are moved in a Cartesian coordinate system aligned with the mean wind. We make this distinction because our profile analysis gives a parameter set consistent with an S profile. The result is that a bLS model based on profile parameters will move particles with an exaggerated horizontal velocity (a profile of speed in the x–y plane spuriously stands in for velocity along x). Because $S > U$, we expect $u_{*\mathrm{pro}} > u_{*\mathrm{son}}$, and this is the case (Fig. 10). This situation affects the turbulent statistics used in the bLS model (which are scaled with u_*).

Given the previous good Q_{bLS} estimates stemming from the sonic anemometer prescriptions, and given the systematic difference between profile and sonic anemometer parameters (Fig. 10), we expect poor results from the profile-based estimates. Yet overall the two estimates are surprisingly similar. For the nine trials in which both sonic anemometer and profile data are available, the average Q_{bLS}/Q is 1.00 using the sonic anemometer parameters and 1.01 using the profile parameters. This agreement hides an important deficiency.

[8] Increasing the averaging interval increases $\sigma_{u,v}/u_*$ because of the inclusion of larger-scale fluctuations. For example, in trial TA3 a 120-min averaging interval increases $\sigma_{u,v}/u_*$ by 20% when compared with 15-min intervals.

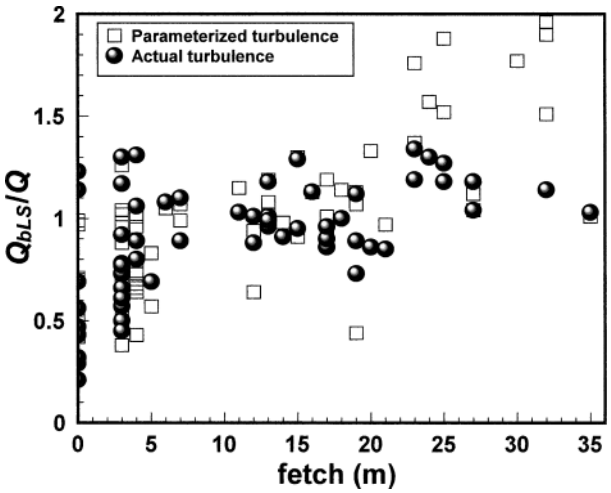

FIG. 11. Ratio of predicted to actual emission rate (Q_{bLS}/Q) using profile-based estimates of u_*, z_0, and L with parameterized turbulence values and actual turbulence values.

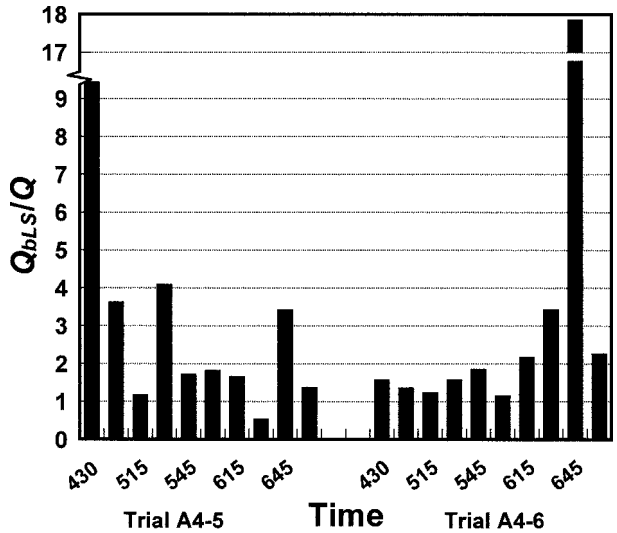

FIG. 12. Ratios of predicted to actual emission rate (Q_{bLS}/Q) vs local time for trials A4-5 and A4-6: a period of MOST failure.

Profile-based Q_{bLS} are too small for the near-source laser paths and too large for the more distant paths (see Fig. 11). We attribute this result to the too-large σ_w in the profile-based simulations caused by a too-large u_{*pro}. This supposition is confirmed by the improved results when we tune $b_{u,v,w}$ in our profile-based simulations to give the proper $\sigma_{u,v,w}$ (Fig. 11).

We conclude that profile-based Q_{bLS} estimates are inferior to sonic anemometer–based estimates. This fact can be blamed on a too-high u_{*pro}, which leads to erroneously high average wind velocities and turbulence levels in our bLS simulation. We believe that the error in u_{*pro} is only partly explained by the difference between U and S. Another factor may be our unsophisticated correction for overspeeding, based on observations only at $z_{son} = 2$ m. A possibility we did not seriously pursue is that our presupposition of $k_v = 0.4$ is incorrect.

c. *Example of a failure (A4)*

Trial A4 represents a period of poor bLS performance. On average, Q_{bLS} overestimates Q by a factor of 3, and, in one 15-min period, it overestimates Q by a factor of almost 18 (Fig. 12). We believe this result is due to the failure of the MOST-based atmospheric description used in the bLS model. This trial spans a sunrise period (0415–0700 local time, sunrise ~0515), during which the skies were clear and winds were light, conditions that are known to be difficult to characterize using MOST (see Wyngaard 1973). This explanation is confirmed by comparing the S and T profiles from the cups and thermocouples with the equivalent MOST profiles derived from the sonic-anemometer u_{*son}, L_{son}, and z_{0son}. Figure 13 shows the poor agreement between the two for the 0515–0530 period, along with a more typical period of good agreement from another trial. Six of the 10 periods from A4 are judged to have similarly inaccurate MOST profiles. Further evidence of the breakdown in MOST is the large period-to-period variability in σ_w/u_* (from 1.0 to 5.6). Given the inability of MOST

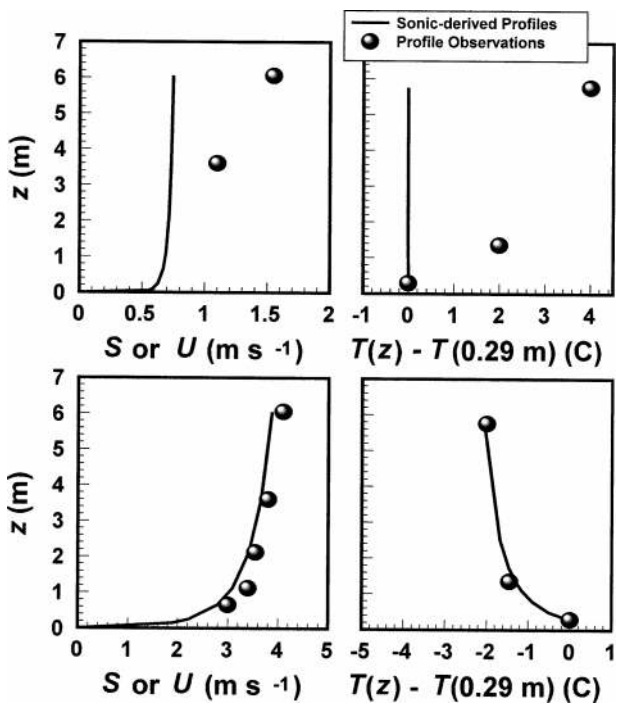

FIG. 13. Average wind velocity U and temperature T predicted from sonic anemometer estimates of u_*, L, and z_0 (solid lines). Profile observations of average wind speed S and T are given by symbols. (top) A 15-min period from trial A4 (MOST failure), and (bottom) a period from trial TA4 (MOST success). Temperature profiles are displayed as the difference between the measured temperature and the value at $z = 0.29$ m.

to describe A4, there is little hope for accurate Q_{bLS} estimates.

How can a user identify periods of MOST failure like A4 and disregard Q_{bLS} during these times? Extreme L has been used to identify problem periods, but some troublesome periods in A4 have a moderate L. Another possibility is to avoid what are qualitatively difficult periods: sunrise and sunset transitions and intervals of near calm. A universal feature of A4 is low u_{*son} (<0.1 m s^{-1}). In fact, over our whole experiment, the diagnostic $u_* \leq 0.15$ m s^{-1} is the single best indicator of inaccurate Q_{bLS}; eliminating these cases results in an average Q_{bLS}/Q of 0.97 and $\sigma_{Q/Q}$ of 0.28. Using u_* as an indicator of the quality of micrometeorological inferences is not unusual (e.g., Massman and Lee 2002). A low u_* is taken to correlate with both large measurement errors and the likelihood of a complex atmospheric state in which assumptions of stationarity and horizontal homogeneity (which underlie MOST) are invalid.

We cannot rule out the possibility that during low winds our methane plume was subject to buoyancy effects at short range; in the lightest winds the pinhole outlet plumes of methane may have remained intact and thus unstably buoyant.

5. Conclusions

When we exclude periods of extreme stratification or MOST failure, the bLS inverse-dispersion technique diagnoses the strength of a small ground-level source with small bias (mean value of Q_{bLS}/Q within 2% of unity). If we also exclude cases in which the detecting laser path lay above or immediately downwind from the source, a circumstance in which the laser path lies at the edge of the gas plume, the period-to-period variability in Q_{bLS} was acceptably small ($\sigma_{Q/Q}$ of order 0.2). This result accords with the known accuracy of Lagrangian stochastic models in simulating short-range dispersion in ideal flow. Using the line-average observation C_L almost certainly enhanced the accuracy with which Q was diagnosed and rendered the experimental procedure very forgiving (we could position the laser and be relatively unconcerned with changing wind direction).

Based on these experiments, we make several recommendations for using a bLS model (or any similar dispersion model based on MOST) to infer Q from an area source in an ideal surface-layer problem.

- Line-average concentration measurement is preferable to a point measurement.
- Avoid making concentration measurements near the edge of the tracer plume; the chosen location should be several height multiples downwind of the edge of the tracer source (e.g., at least $10z_m$ from the upwind source edge).
- Distance of the detector from the source should be small enough that the concentration rise over background is accurately measured.
- It would be ideal to use traditional micrometeorological averaging times of 10–30 min in calculating concentration and meteorological statistics.
- Periods of extreme atmospheric stability should not be used in assessing Q_{bLS}.
- Disregard periods of low u_* (e.g., $u_* \leq 0.15$ m s^{-1}).

An important research question is: How far can we move away from an ideal surface-layer problem and yet retain the accuracy of a simple bLS technique based on MOST? The theoretical study of Wilson et al. (2001b) looked at this issue in a lagoon setting in which the aerodynamic environment evolves as the wind moves from the upwind land surface to a smoother and warmer/cooler lagoon surface. They found that bLS estimates of Q from the lagoon, inferred with a MOST-based bLS model, were relatively insensitive to the aerodynamic modifications induced by the lagoon. This result is encouraging, because it suggests robustness to nonideal locations.

A prime motive of our study was to have it serve as preparation to examine this issue of bLS robustness in nonideal settings. We have demonstrated the accuracy of a Q_{bLS} measurement system in ideal conditions. The next phase of our work is to introduce a dramatic wind field ''disturbance'' in the environment around our synthetic source. Can a Q_{bLS} prediction based on a MOST description of the atmosphere that is clearly inappropriate still be useful?

Acknowledgments. This work has been supported by research grants from the Natural Sciences and Engineering Research Council of Canada (NSERC) and the Canadian Foundation for Climate and Atmospheric Sciences (CFCAS). The useful comments of anonymous reviewers were appreciated.

APPENDIX

Windflow Parameterization

a. Average wind velocity U

Aligning x with the mean surface wind ensures $V = 0$. We use the diabatically corrected logarithmic wind profile to calculate

$$U = \frac{u_*}{k_v}\left[\ln\left(\frac{z}{z_0}\right) + \psi\left(\frac{z}{L}\right)\right]. \tag{A1}$$

Here, k_v is von Kármán's constant (taken as 0.4), ψ is a Monin–Obuhkhov universal function, and L is the Obukhov stability length. We specified ψ as (Dyer 1974; Paulson 1970)

$$\psi = \begin{cases} \dfrac{4.8z}{L} & (\text{for } L > 0) \quad \text{and} \\ -2\ln\left(\dfrac{1+\alpha}{2}\right) - \ln\left(\dfrac{1+\alpha^2}{2}\right) + 2\tan^{-1}(\alpha) - \dfrac{\pi}{2} \\ \qquad (\text{for } L < 0), \end{cases} \tag{A2}$$

where $\alpha = (1 - 16z/L)^{1/4}$.

b. Velocity fluctuations

We make the traditional surface-layer assumption that the standard deviation of the vertical velocity scales on u_* and takes the form

$$\sigma_w = b_w u_* \varphi_w, \tag{A3}$$

where b_w is a scaling constant and φ_w is a stability correction function. We use

$$\varphi_w = \begin{cases} 1 & (\text{for } L > 0) \quad \text{and} \\ \left(1 - 3\dfrac{z}{L}\right)^{1/3} & (\text{for } L < 0). \end{cases} \tag{A4}$$

The latter formula was taken from Panofsky et al. (1977). In stable and neutral stratification, we assumed height independence of the horizontal fluctuations:

$$\sigma_u = b_u u_* \quad \text{and} \quad \sigma_v = b_v u_*. \tag{A5}$$

In unstable stratification, these fluctuations depend on the degree of stability. We adapted a formula for σ_v^2, given by Gryning et al. (1987), with $z/h = 0$, to give continuity with Eq. (A5):

$$\sigma_u^2 = b_u^2 u_*^2 + 0.35 w_*^2 \quad \text{and}$$
$$\sigma_v^2 = b_v^2 u_*^2 + 0.35 w_*^2, \tag{A6}$$

where w_* is the convective velocity scale ($w_* \to 0$ as $L \to -\infty$):

$$w_* = \left(-\frac{u_*^3 h}{L k_v}\right)^{1/3}, \tag{A7}$$

where h is the depth of the unstable boundary layer. In calculating w_*, we assume $h = 1000$ m. These formulas for σ_u and σ_v are similar to those given by Panofsky et al. (1977). In very unstable conditions, h is important in determining σ_u and σ_v, but in most applications it is unknowable, which therefore limits our bLS accuracy.

We used $b_{u,v,w}$ of 2.5, 2.0, and 1.25 except where indicated. These commonly accepted values were seen to describe our Ellerslie measurements reasonably well (see Fig. A1).

c. Dissipation rate

The turbulent kinetic energy dissipation rate ε is usually assumed to be proportional to u^3 and to vary with height and stability. We take the following form for ε:

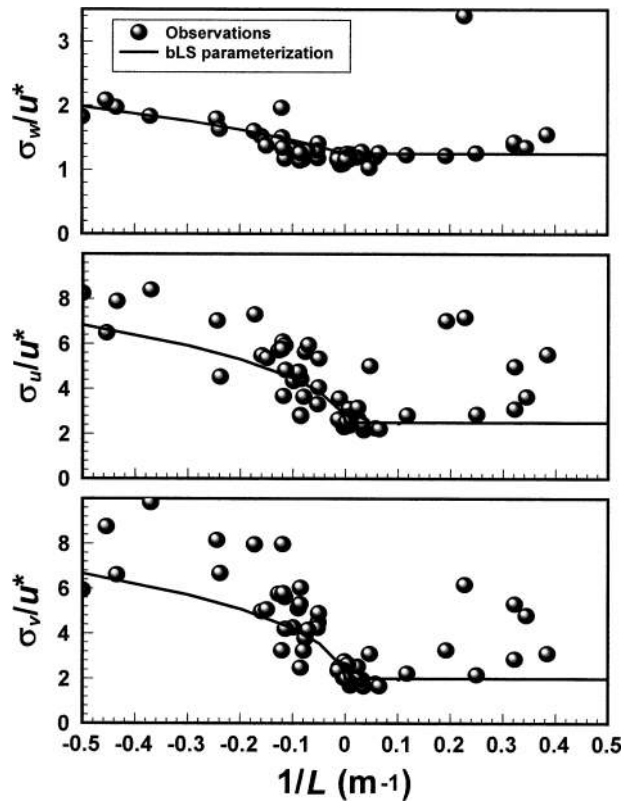

FIG. A1. The standard deviation of turbulent fluctuations $\sigma_{u,v,w}$ scaled on friction velocity u_* vs the Obukhov length L as measured by our sonic anemometer at $z_{son} \approx 2$ m (symbols). The lines are formulas used in our bLS model [Eqs. (A3)–(A6)].

$$\varepsilon = \frac{u_*^3}{k_v z}\varphi_\varepsilon, \tag{A8}$$

where φ_ε is a stability correction factor ($\varphi_\varepsilon = 1$ in neutral stability). We chose φ_ε so that the far-field diffusivity of our bLS model, as calculated following Sawford and Guest (1988), was consistent with the LS model of Wilson et al. (1981), validated on Project Prairie Grass. That model, unlike ours, defined a Lagrangian time scale with a stability correction function φ_L. Equal diffusivities between these models requires

$$\frac{2}{C_0\varepsilon}(\sigma_w^4 + u_*^4) = Az\sigma_w\varphi_L, \tag{A9}$$

where A is the scaling constant for the Lagrangian time scale given by Wilson et al. ($A = 0.5$). Substituting $b_w\varphi_w$ for σ_w/u_* and rearranging Eq. (A9) gives

$$C_0\varepsilon = \frac{2k_v}{A}\frac{b_w^4\varphi_w^4 + 1}{b_w\varphi_w\varphi_L}\frac{u_*^3}{k_v z}. \tag{A10}$$

Equations (A9) and (A8) are satisfied by defining

$$C_0 = \frac{2k_v}{A}\left(\frac{b_w^4 + 1}{b_w}\right) \quad \text{and} \tag{A11}$$

$$\varphi_\varepsilon = \frac{b_w^4\varphi_w^4 + 1}{(b_w^4 + 1)\varphi_w\varphi_L}. \tag{A12}$$

Using the φ_L formulas given by Wilson et al. and the φ_w formulas in Eq. (A4) yields

$$\varphi_\varepsilon = \begin{cases} 1 + 5z/L & (\text{for } L > 0), \\ \dfrac{b_w^4(1 - 3z/L)^{1.33} + 1}{(b_w^4 + 1)(1 - 3z/L)^{0.33}(1 - 6z/L)^{0.25}} & (\text{for } L < 0). \end{cases} \tag{A13}$$

With $b_w = 1.25$, this gives φ_ε values similar to the formulas proposed by Wyngaard and Cote (1971). With $A = 0.5$ and $b_w = 1.25$, we find $C_0 = 4.41$. The turbulent Schmidt number (Sc) of our model is Sc = 0.64 in neutral conditions (see Flesch et al. 2002).

REFERENCES

Argete, J. C., and J. D. Wilson, 1989: The microclimate in the center of small square sheltered plots. *Agric. For. Meteor.,* **48,** 185–199.

Carter, R. E., and Coauthors, 1993: A method of predicting point and path averaged ambient air VOC concentrations using meteorological data. *J. Air Waste Manage. Assoc.,* **43,** 480–488.

Dyer, A. J., 1974: A review of flux-profile relationships. *Bound.-Layer Meteor.,* **7,** 363–372.

Flesch, T. K., J. D. Wilson, and E. Yee, 1995: Backward-time Lagrangian stochastic dispersion models, and their application to estimate gaseous emissions. *J. Appl. Meteor.,* **34,** 1320–1332.

——, J. H. Prueger, and J. L. Hatfield, 2002: Turbulent Schmidt number from a tracer experiment. *Agric. For. Meteor.,* **111,** 299–307.

Garratt, J. R., 1992: *The Atmospheric Boundary Layer*. Cambridge University Press, 316 pp.

Gryning, S. E., A. A. M. Holtslag, J. S. Irwin, and B. Sivertsen, 1987: Applied dispersion modelling based on meteorological scaling parameters. *Atmos. Environ.,* **21,** 79–89.

Hartley, D., and R. Prinn, 1993: Feasibility of determining surface emissions of trace gases using an inverse method in a 3-dimensional chemical transport model. *J. Geophys. Res.,* **98,** 5183–5197.

Kaharabata, S. K., P. H. Schuepp, and R. L. Desjardins, 2000: Source strength determination of a tracer gas using an approximate solution to the advection–diffusion equation for microplots. *Atmos. Environ.,* **34,** 2343–2350.

Kaimal, J. C., and J. J. Finnigan, 1994: *Atmospheric Boundary Layer Flows: Their Structure and Measurement*. Oxford University Press, 289 pp.

Massman, W. J., and X. Lee, 2002: Eddy covariance flux corrections and uncertainties in long-term studies of carbon and energy exchanges. *Agric. For. Meteor.,* **113,** 121–144.

Panofsky, H. A., H. Tennekes, D. H. Lenschow, and J. C. Wyngaard, 1977: The characteristics of turbulent velocity components in the surface layer under convective conditions. *Bound.-Layer Meteor.,* **11,** 355–361.

Paulson, C. A., 1970: The mathematical representation of wind speed and temperature profiles in the unstable atmospheric surface layer. *J. Appl. Meteor.,* **9,** 857–861.

Raupach, M. R., 1989: A practical Lagrangian method for relating scalar concentrations to source distributions in vegetative canopies. *Quart. J. Roy. Meteor. Soc.,* **115,** 609–632.

Rodean, H. C., 1996: *Stochastic Lagrangian Models of Turbulent Diffusion. Meteor. Monogr.,* No. 48, Amer. Meteor. Soc., 84 pp.

Sawford, B. L., and F. M. Guest, 1988: Uniqueness and universality of Lagrangian stochastic models of turbulent dispersion. Preprints, *Eighth Symp. on Turbulence and Diffusion,* San Diego, CA, Amer. Meteor. Soc., 96–99.

Seibert, P., 1999: Inverse modelling of sulfur emissions in Europe based on trajectories. *Inverse Methods in Global Biogeochemical Cycles, Geophys. Monogr.,* No. 114, Amer. Geophys. Union, 147–154.

Thomson, D. J., 1987: Criteria for the selection of stochastic models of particle trajectories in turbulent flows. *J. Fluid Mech.,* **180,** 529–556.

Wilson, J. D., and B. L. Sawford, 1996: Review of Lagrangian stochastic models for trajectories in the turbulent atmosphere. *Bound.-Layer Meteor.,* **78,** 191–210.

——, G. W. Thurtell, and G. E. Kidd, 1981: Numerical simulation of particle trajectories in inhomogeneous turbulence, III. Comparison of predictions with experimental data for the atmospheric surface-layer. *Bound.-Layer Meteor.,* **21,** 443–463.

——, ——, ——, and E. G. Beauchamp, 1982: Estimation of the rate of gaseous mass transfer from a surface source plot to the atmosphere. *Atmos. Environ.,* **16,** 1861–1867.

——, T. K. Flesch, and R. d'Amours, 2001a: Surface delays for gases dispersing in the atmosphere. *J. Appl. Meteor.,* **40,** 1422–1430.

——, ——, and L. A. Harper, 2001b: Micrometeorological methods for estimating surface exchange with a disturbed windflow. *Agric. For. Meteor.,* **107,** 207–225.

Wyngaard, J. C., 1973: On surface layer turbulence. *Workshop on Micrometeorology,* D. A. Haugen, Ed., Amer. Meteor. Soc., 101–149.

——, and O. R. Cote, 1971: The budgets of turbulent kinetic energy and temperature variance in the atmospheric surface layer. *J. Atmos. Sci.,* **28,** 190–201.